Natural Speed Observer for Nonsalient AC Motors

Jiahao Chen, *Member, IEEE,* Jie Mei, *Member, IEEE,* Xin Yuan, *Member, IEEE,*
Yuefei Zuo, *Member, IEEE,* Christopher H. T. Lee, *Senior Member, IEEE*

***Abstract*—This letter addresses experimental validation of the reduced-order natural speed observer design for position sensorless drive with nonsalient permanent magnet synchronous motor. The natural speed observer and the active flux estimator are connected in a cascaded fashion, which results in a simple sensorless algorithm that needs only to tune one bandwidth parameter for flux estimation and one bandwidth parameter for speed observation. Experimental results of high speed reversal test, zero speed stopping test and slow speed reversal test are included, where the practice of applying non-zero d-axis current at zero speed has shown to be effective for loaded zero speed stopping test, but it causes zero-speed locked-up at slow speed reversal with acceleration rate of 50 rpm/s. Four remedies are compared to improve the slow speed reversal test and the proposed method gives almost ramp actual speed waveform, non-diverging q-axis current and smooth transition in position waveform during zero speed crossing. A new dynamic expression of the active flux is proposed and with the aid of the active flux concept, the proposed sensorless algorithm is also applicable to various types of ac motors.**

***Index Terms*—permanent magnet motor drives, sensorless control, review, active flux, unified model.**

NOMENCLATURE

Let p denote the differentiation operator, u_d, u_q denote the d-axis, q-axis voltages, i_d, i_q denote d-axis, q-axis currents, L_d, L_q designate the d-axis, q-axis inductances, ω the electrical synchronous angular speed, ω_r the electrical rotor angular speed, R the stator resistance, $K_E \in \mathbb{R}_+$ the permanent magnet flux linkage, J_s the shaft inertia, $T_{\rm em}$ the electromagnetic torque, T_L the load torque, $n_{\rm pp}$ the pole pair number, and finally, $\boldsymbol{J}=\left[\begin{smallmatrix}0 & -1\\ 1 & 0\end{smallmatrix}\right]$, $\boldsymbol{I}=\left[\begin{smallmatrix}1 & 0\\ 0 & 1\end{smallmatrix}\right]$.

This letter also uses *bold* vector notations for α-β frame quantities, such as stator current $\boldsymbol{i} = [i_\alpha, i_\beta]^{\mathsf{T}}$, stator voltage $\boldsymbol{u} = [u_\alpha, u_\beta]^{\mathsf{T}}$, (extended) emf $\boldsymbol{e} = [e_\alpha, e_\beta]^{\mathsf{T}}$, and rotor active flux (linkage) $\boldsymbol{\psi}_r = [\psi_{\alpha r}, \psi_{\beta r}]^{\mathsf{T}}$.

I. SENSORLESS DRIVE REVIEW: A NEW PERSPECTIVE

THE LITERATURE of sensorless motor drives has been developed for decades, and there has been a trend of unifying sensorless control for different motor types [1]–[3]. When it comes to literature review of different sensorless drives, the widely accepted classification is to divide sensorless drives into model based drives and magnetic asymmetry based drives (see, e.g., [4], [5]). This letter, however, attempts to provide a new perspective in terms of how speed estimation and position estimation are related, and to categorize the existing sensorless drives into groups of three design patterns.

A. Coupled Position and Speed Acquisition

The first design pattern is to get both speed estimate $\hat{\omega}$ and rotor d-axis position estimate $\hat{\theta}_d$ from one full-order observer. This relies on the fact that both $\hat{\omega}$ and $\hat{\theta}_d$ can be obtained from observer's output error, i.e., estimated current error—more specifically, $\hat{\omega}$ from q-axis current error, and $\hat{\theta}_d$ from d-axis current error [6]. Typical example is the direct field oriented controlled sensorless induction motor drive [7]. There are only a few papers in the field of sensorless permanent magnet (PM) motor drives that follow this design pattern. For example, reference [8] adopts model reference adaptive system (MRAS) as a filter to the switching terms of a sliding mode observer (SMO) to get both position and speed, while a recent one [9] devises speed adaptive full-order observer based on extended emf model and elaborates its gain design with the aid of linear system tools.

The observer designs that are previously applied to induction motors should also be applicable to synchronous motors. For example, motivated by the "known regressor model" in [10], we can replace extended emf $\boldsymbol{e}$ with a new state variable $\boldsymbol{\chi} = -\boldsymbol{e} - \omega \boldsymbol{J} L_d \boldsymbol{i}$. This results in new PM motor dynamics in which the regressor of speed consists of known signals:

$$\begin{aligned} L_d p\boldsymbol{i} &= \boldsymbol{u} - R\boldsymbol{i} + \boldsymbol{\chi} + (2L_d - L_q)\,\omega \boldsymbol{J}\boldsymbol{i} \\ p\boldsymbol{\chi} &= -\omega \boldsymbol{J}(\boldsymbol{u} - R\boldsymbol{i}) + \omega^2 (L_d - L_q)\boldsymbol{i} \end{aligned} \tag{1}$$

for which one can design speed adaptive high gain observer [11] or speed update rule with filtered regressor [10] to get $\hat{\omega}$, and at the same time obtains $\hat{\theta}_d$ from the estimate of $\boldsymbol{\chi}$.

B. Position Independent Speed Acquisition

The second design pattern is to first estimate speed $\hat{\omega}$ and then calculate rotor d-axis position with an integrator as $\hat{\theta}_d = \frac{1}{p}\left(\hat{\omega} + \omega^*_{\rm sl}\right)$, with $\omega^*_{\rm sl}$ the commanded slip angular speed. Typical examples include the sensorless indirect field oriented controlled, PM motor drive (with $\omega^*_{\rm sl} = 0$) [12], [13] and induction motor drive (see e.g., [10], [14]). Particularly, for the emf based drives [12]–[14], the calculated speed signal using calculated emf $\hat{\boldsymbol{e}}$ needs to be embedded in a low pass filter to resolve algebraic loop problems, as is discussed in [2].

C. Speed Independent Position Acquisition

The third design pattern is exclusively targeted for synchronous motors (i.e., PM and synchronous reluctance motors) as it directly estimates the rotor d-axis position $\hat{\theta}$ from which the speed information $\hat{\omega}$ is later extracted. Typical examples include high frequency signal injection based drives [15], emf based drives [1], [4], [16] and flux based drives [3], [17].

The high frequency injection method estimates $\hat{\theta}_d$ utilizing the *rotor saliency* on the q-axis using invasive injection of high frequency voltage. The resulting practical issues such as limited current control bandwidth and audible noise can be resolved by increasing injection frequency to PWM frequency [15], while the theoretical development can be found in [18].

The active flux can be defined in complex notations as $\boldsymbol{\psi}_r = K_{\rm Active} \mathrm{e}^{j\theta_d}$, with $K_{\rm Active} = K_E + (L_d - L_q)\, i_d$. Extended emf is defined as $\boldsymbol{e} = [\omega K_{\rm Active} - (L_d - L_q)\, p i_q]\, \mathrm{e}^{j\theta_d}$, and it becomes $\omega \boldsymbol{\psi}_r$ if $p i_q = 0$, e.g., at steady state.

For salient PM motors, the extended emf $\boldsymbol{e}$ was estimated by Gopinath reduced-order observer [1]. For non-salient PM motors, the emf was estimated by SMO [4], [8], [16].

The dynamics of active flux involve pure integration, which are also known as the critical stable voltage model in induction motor drive context. Stabilizing the active flux estimation is a popular topic, some recent development in the PM motor drive context, will be briefly reviewed here. As a contribution from the control community, in [5], the stator flux estimator was corrected by the squared PM flux amplitude error, of which the stability property was found to be distinct at different speeds. While in electrical engineering community, a disturbance observer was designed to estimate the presumed low frequency disturbance in the presumed "sinusoidal" flux model, using only voltage model [17]. This work is followed in [19] to further incorporate current model information, and in [20] to cope with discretization error.

With the information of θ_d, $\boldsymbol{e}$, or $\boldsymbol{\psi}_{\rm Active}$ available, a speed estimator is then devised, e.g., Luenberger observer [15], I&I technique [5], $\boldsymbol{e}$-MRAS [1], [16], adaptive observer based on the dq frame voltage model [21], phase-locked-loop (PLL) [3] and type-2 system [17].

It is worth mentioning that the $\hat{\theta}_d$ estimation process in [1], [17] "weakly" depends on the estimated speed $\hat{\omega}$. To show or reduce speed dependency of position estimation, it has been shown with frequency analysis in [17] that an erroneous speed is not a big issue for active flux estimation, while in [1], the H_∞ norm of the transfer function from estimated speed error to extended emf error is minimized by properly placing observer poles.

D. Contribution of This Letter

The contribution of this letter is twofold. First, by following the third design pattern, to propose and experimentally validate a motor motion dynamics based speed observer with the aid of natural observer concept and active flux concept. The 4th-order active flux estimator gives $\hat{\theta}_d$ without knowledge of $\hat{\omega}$; and by using $\hat{\theta}_d$, a 3rd-order reduced-order natural speed observer potentially provides consistent estimate of $\hat{\omega}$ even during speed transient conditions. The proposed sensorless scheme is simple to implement with only two tuning parameters, and has potential for high performing sensorless motor drive as it removes the constant speed assumption. Second, a new dynamic expression is proposed for active flux $K_{\rm Active}$, which is crucial for further generalizing our proposed method to be applicable to various types of ac motors.

II. Nonsalient Motor Model in dq Frame

The "3rd-order" dynamics of a nonsalient ac motor in rotor field oriented synchronous d-q frame are:

$$u_d = R i_d + L_q\,(p i_d - \omega i_q) + p K_{\rm Active} \tag{2a}$$

$$u_q = R i_q + L_q\,(p i_q + \omega i_d) + \omega K_{\rm Active} \tag{2b}$$

$$\frac{J_s}{n_{\rm pp}} p\omega_r = \underbrace{\tfrac{3}{2} n_{\rm pp} K_{\rm Active} i_q}_{T_{\rm em}} - T_L \tag{2c}$$

where the rotor flux (i.e., active flux) is determined as follows

$$K_{\rm Active} = \frac{1}{\frac{(L_d - L_q)}{r_{\rm req}} p + 1}\,(L_d - L_q)\, i_d + K_E \tag{3}$$

and all other symbols are defined in Nomenclature.

Model (2), (3) describes a wound field synchronous motor with a short-circuited damper winding to allow self-starting, if we let $K_E \propto i_f$ with i_f as the field winding current [22].

For PM motors and synchronous reluctance motors, $\omega = \omega_r$, and rotor resistance $r_{\rm req}$ is ∞[1], so (3) reduces to $K_{\rm Active} = (L_d - L_q)\, i_d + K_E$ [3].

For induction motors, $K_E = 0$ and $L_d - L_q$ is redefined as the magnetizing inductance in inverse Γ circuit[2], and (3) becomes $p K_{\rm Active} = -\frac{L_d - L_q}{r_{\rm req}} K_{\rm Active} + r_{\rm req} i_d$.

III. Reduced-order Natural Speed Observer with Active Flux Concept

A. The Natural Speed Observer

The natural observer originated in [24] is applicable to dc motor and ac induction motor. By noticing the fact that the nonsalient motor model in dq frame is identical to that of a dc motor, we propose the 3rd-order reduced-order natural speed observer that is simply a copy of (2b) and (2c) plus a load torque identifier:

$$L_q p\hat{i}_q = u_q - R\hat{i}_q - \hat{\omega}\,(L_q i_d + K_{\rm Active}) \tag{4a}$$

$$p\hat{\omega}_r = J_s^{-1} n_{\rm pp} \left[\tfrac{3}{2} n_{\rm pp} K_{\rm Active} \hat{i}_q - \hat{T}_L\right] \tag{4b}$$

$$\hat{T}_L = K_P \varepsilon + K_I \frac{1}{p} \varepsilon + K_D p \varepsilon \tag{4c}$$

where $K_P, K_I, K_D \in \mathbb{R}_+$, a hat $\hat{}$ at the top of a symbol indicates estimated value, and ε is the active power error

$$\varepsilon = |u'_q| \left(i_q - \hat{i}_q\right) \tag{5}$$

when $u'_q = u_q$. The implementation of (4) and (5) relies on the information of rotor d-axis position $\hat{\theta}_d$, to calculate the dq frame quantities:

$$\begin{aligned} i_d &= i_\alpha \cos\hat{\theta}_d + i_\beta \sin\hat{\theta}_d \\ i_q &= -\,i_\alpha \sin\hat{\theta}_d + i_\beta \cos\hat{\theta}_d \\ u_q &= -\,u_\alpha \sin\hat{\theta}_d + u_\beta \cos\hat{\theta}_d \end{aligned} \tag{6}$$

The observer (4) is intuitive when applied to PM motors, whereas we need to add the slip relation: $\hat{\omega} = r_{\rm req} \frac{i_q}{K_{\rm Active}} + \hat{\omega}_r$ before it can be applied to induction motors.

The stability of the time-varying system, (4) and (5), can be proved via finding Lyapunov function using Krasovskii's stability technique [23]. However, if we treat it as a time-invariant system by assuming $K_{\rm Active}$, i_d and u'_q are constants, we can instead, analyze (4) through the transfer function from disturbance, T_L, to output error, $i_q - \hat{i}_q$

$$\frac{(i_q - \hat{i}_q)\,(p)}{T_L\,(p)} = \frac{p}{(p + \omega_{\rm ob})^3} \frac{n_{\rm pp}}{L_q J_s}\,(L_q i_d + K_{\rm Active}) \tag{7}$$

[1]The unified model in [2], however, needs to put $r_{\rm req} = 0$ for PM motors.

[2]To be specific, following the inverse-Γ circuit notations in [23], $L_q \triangleq L_\sigma$ is the total leakage inductance, and $L_d \triangleq L_\mu + L_\sigma$ is the stator inductance.

This article has been accepted for publication in a future issue of this journal, but has not been fully edited. Content may change prior to final publication. Citation information: DOI 10.1109/TPEL.2021.3094583, IEEE Transactions on Power Electronics

where we have tuned the PID coefficients to place the three observer poles at $-\omega_{\rm ob} \in \mathbb{R}_{<0}$

$$\begin{cases} 3\omega_{\rm ob} = \frac{n_{pp}}{L_q J_s}\left(L_q i_d + K_{\rm Active}\right) K_D \left|u_q'\right| + \frac{R}{L_q} \\ 3\omega_{\rm ob}^2 = \frac{n_{pp}}{L_q J_s}\left(L_q i_d + K_{\rm Active}\right)\left(\frac{3}{2} n_{pp} K_{\rm Active} + K_P \left|u_q'\right|\right) \\ \omega_{\rm ob}^3 = \frac{n_{pp}}{L_q J_s}\left(L_q i_d + K_{\rm Active}\right) K_I \left|u_q'\right| \end{cases} \tag{8}$$

However, with $u_q' = u_q$, u_q' becomes a time-varying function of speed ω_r, and this has made (8) not feasible for variable speed operation. To make tuning rule (8) time-invariant with regard to speed changes, we propose to use q-axis current error as ε, by putting $u_q' = 1$.

B. The Active Flux Estimator for Acquiring $\hat{\theta}_d$

The adopted flux estimator in the PM motor context is

$$p\boldsymbol{\psi}_1 = \boldsymbol{u} - R\boldsymbol{i} + \boldsymbol{w}_v + \left(k_p + \frac{k_i}{p}\right)\left(K_{\rm Active}\frac{\boldsymbol{\psi}_2}{|\boldsymbol{\psi}_2|} - \boldsymbol{\psi}_2\right) \tag{9}$$

where stator flux estimate is $\boldsymbol{\psi}_1 = [\psi_{\alpha 1}, \psi_{\beta 1}]^{\mathsf{T}}$, the rotor active flux estimate is $\boldsymbol{\psi}_2 = \boldsymbol{\psi}_1 - L_q\boldsymbol{i}$, and the disturbance is denoted by $\boldsymbol{w}_v \in \mathbb{R}^2$. In this estimator, only the amplitude of flux estimate is corrected by the active flux amplitude parameter $K_{\rm Active}$. Then, the $\hat{\theta}_d$ is computed as $\arctan 2\left(\psi_{\beta 2}, \psi_{\alpha 2}\right)$.

If we designate two auxiliary rotor active flux estimates as voltage model ($\boldsymbol{\psi}_{\rm VM}$) and current model ($\boldsymbol{\psi}_{\rm CM}$) to satisfy

$$\begin{aligned} \boldsymbol{\psi}_{\rm CM} &= K_{\rm Active}\boldsymbol{\psi}_2 |\boldsymbol{\psi}_2|^{-1} \\ p\left(\boldsymbol{\psi}_{\rm VM} + L_q\boldsymbol{i}\right) &= \boldsymbol{u} - R\boldsymbol{i} + \boldsymbol{w}_v \end{aligned} \tag{10}$$

we can express the flux estimate from (9) in terms of $\boldsymbol{\psi}_{\rm VM}$ and $\boldsymbol{\psi}_{\rm CM}$ as follows (see also [19])

$$\boldsymbol{\psi}_2 = \frac{k_p p + k_i}{p^2 + k_p p + k_i}\boldsymbol{\psi}_{\rm CM} + \frac{p^2}{p^2 + k_p p + k_i}\boldsymbol{\psi}_{\rm VM} \tag{11}$$

and we can also derive the transfer function from the disturbance $\boldsymbol{w}_v$ to flux mismatch $\boldsymbol{\psi}_2 - \boldsymbol{\psi}_{\rm CM}$ as

$$\left(\boldsymbol{\psi}_2 - \boldsymbol{\psi}_{\rm CM}\right) = \frac{p}{p^2 + k_p p + k_i}\boldsymbol{w}_v \tag{12}$$

From (11) and (12), k_p, k_i can be tuned by placing the poles of the second-order systems via the relations: $k_p = 2\omega_{\rm est}\zeta_{\rm est}$ and $k_i = \omega_{\rm est}^2$, where $\zeta_{\rm est}$ is the damping ratio and $\omega_{\rm est}$ is the undamped natural frequency. In addition, the relation among $\boldsymbol{\psi}_{\rm VM}$, $\boldsymbol{\psi}_{\rm CM}$, and $\boldsymbol{\psi}_2$ is clarified in Fig. 1b.

Please note the above analysis does not make any conclusion regarding the convergence to actual flux. In order to prove the stability of the estimated flux error $\boldsymbol{\psi}_r - \boldsymbol{\psi}_2$, a fourth order dynamical system with $\boldsymbol{\psi}_r - \boldsymbol{\psi}_{\rm CM}$ and $\boldsymbol{\psi}_{\rm CM} - \boldsymbol{\psi}_2$ as states must be analyzed using a similar approach elaborated in [25].

C. Brief Summary

The implementation of the proposed sensorless algorithm is summarized by the block diagram in Fig. 1a. In Fig. 1a, the voltage $\boldsymbol{u}$ is substituted with the voltage command $\boldsymbol{u}^*$, and the current $\boldsymbol{i}$ is obtained by applying amplitude invariant Clarke transformation to measured phase currents. Then, $\boldsymbol{u}$ and $\boldsymbol{i}$ are the inputs to the flux estimator (9), as shown in Fig. 1b, which outputs $\boldsymbol{\psi}_2$ to provide its angle information as $\hat{\theta}_d = \arctan 2\left(\psi_{\beta 2}, \psi_{\alpha 2}\right)$. Rotor position estimate $\hat{\theta}_d$ is used for Park transformation and the resulting dq frame signals i_d, i_q, u_q are the inputs to the speed observer (4) that outputs $\hat{\omega}_r$ for speed control.

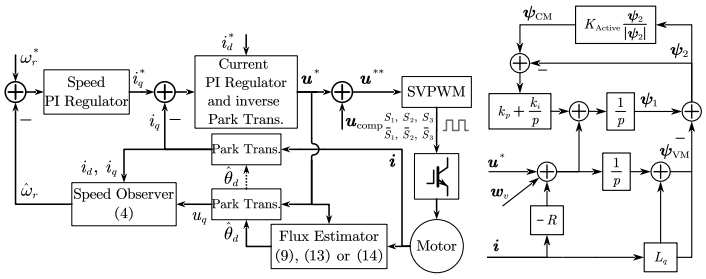

Fig. 1. Block diagram of (a) the proposed position sensorless control system, and (b) the active flux estimator (9).

The tuning process of (9) and (4) is rather simple. First, tune the flux estimator (9) as a second-order system via pole placement using $\omega_{\rm est}$ and $\zeta_{\rm est} = 1$, and then tune the speed observer (4) as a third-order system via pole placement using $\omega_{\rm ob}$.

IV. Experimental Results

The test motor is a 750 W, 3 Arms, 2.4 Nm, 750 rpm[3] (at 50 Hz), $n_{\rm pp} = 4$ pole pair, surface mounted PM motor, and its parameters are: $R = 1.9\ \Omega$, $L_d = L_q = 5.0$ H, $K_E = 0.10$ Wb and $J_s = 7.5\ {\rm kg}\cdot{\rm cm}^2$. The test motor is driven by a voltage source SiC inverter that receives gate signals from the digital signal processor (DSP), TMS320-F28377D. The carrier signal frequency of the space vector pulse width modulation is 10 kHz, and the current sampling period and code execution period are 1×10^{-4} s. The DSP has two cores, one is for implementing control algorithm, and the other is used to generate 6 channels of digital-to-analog (DAC) signals that will be captured by a scope. A dc power supply is used as the dc bus. An encoder with 2500 ppr is used for verification purpose. Current loop bandwidth is tuned to be 200 Hz, the bandwidth of the closed loop speed control is 40 Hz, and speed loop execution period is 5×10^{-4} s.

A. Voltage Error Issues

The active flux estimate $\boldsymbol{\psi}_{\rm Active}$ is prone to be erogenous due to voltage error at low speeds, so it is important to remove the drift in dc bus voltage measurement as well as compensate inverter nonlinearity.

When measuring the inverter's voltage and current characteristics at standstill, it should be emphasized that instead of applying α-axis current, the dc current should be applied at β-axis such that the phase U current (i.e., i_α) is null and phase V and phase W have the same current amplitude with opposite signs. Otherwise, by regulating i_α, the current amplitude of phase U is two times as large as the amplitude of phase V or W, so the distorted phase voltage that is a nonlinear function of phase current cannot be acquired. Finally, multiplying a scaling factor of $\sin(\frac{-2\pi}{3})$ to β-axis quantities gives phase quantities.

[3]In this letter, rpm means mechanical revolution per minute.

This article has been accepted for publication in a future issue of this journal, but has not been fully edited. Content may change prior to final publication. Citation information: DOI 10.1109/TPEL.2021.3094583, IEEE Transactions on Power Electronics

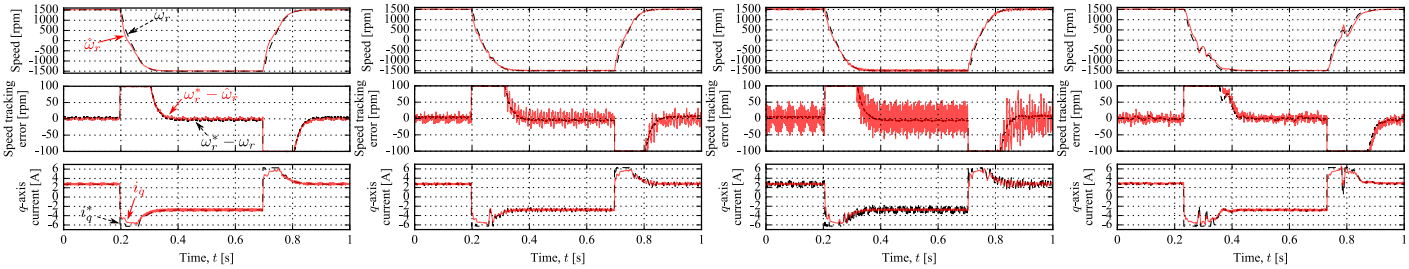

Fig. 2. Sensorless high speed reversal test using (a) $\omega_{\rm ob}=170$; (b) $\omega_{\rm ob}=340$; (c) $\omega_{\rm ob}=510$; (d) SMO from [4] with $k=400$, $\tau_c^{-1}=\frac{|\hat{\omega}_r|}{20}+10$ and PLL with proportional gain of 1000 and integral gain of 1×10^5 (all in SI units).

B. Load Motor Manipulation

The shaft of the test motor is coupled with another servo motor as load. The load motor is controlled with some speed command and its speed loop output limit is set to 2.1 A.

In Fig. 2, the speed command for the load motor is 0 rpm, so the q-axis current has the same sign of the speed at steady state. The overall load torque that includes friction is estimated to be about 1.5 Nm, which equals 62.5% of the motor rated torque.

In Fig. 3 and Fig. 5, in order to test the sensorless drive for various operating conditions, the speed command of the load motor is set to -300 rpm. This means that when the speed is positive, the test motor is motoring; while the test motor is regenerating when the speed is negative. In addition, it is observed that the steady state value of i_q is higher for positive speed operation and is lower in negative speed operation in Fig. 6c, because the load motor "helps" to fight against the friction as long as rotor shaft is spinning at a negative speed.

C. Natural Speed Observer based Sensorless Drive

1) Sensorless High Speed Reversal: Fix $\omega_{\rm est}=25$ rad/s and $\zeta_{\rm est}=1$. Three sets of $\omega_{\rm ob}$ values are tested. According to Fig. 2a, 2b, 2c, the 0%–0.97% rising time for the motor to step from -1500 rpm to 1400 rpm is about 0.12 s regardless of $\omega_{\rm ob}$ values, implying that the speed observer bandwidth is not the bottleneck for reducing rising time. There exists undesired oscillation in $\hat{\omega}_r$ when $\omega_{\rm ob}$ is too large, which leads to oscillated i_q^* and i_q profiles in Fig. 2c. The above results validate the effectiveness of the one parameter speed observer tuning rule (8).

2) Extreme Low Speed Tuning Guidelines: For extreme low speed operation, we recommend to select a large damping ratio $\zeta_{\rm est}$ such that the transfer function in (12) behaves as a first-order one, e.g., no overshoot. According to our studies, we adopt $\zeta_{\rm est}=5$ and $\omega_{\rm est}=2$ rad/s.

3) Sensorless Zero Speed Stopping Test: In order to stabilize zero speed operation when the motor is loaded, we propose to excite the motor with d-axis current, i.e., $i_d=2$ A. Note this nonzero i_d is not an effort to "mitigate" the influence of the inverter nonlinearity, as the motor is loaded and i_q is large. The reason is that, in a detuned controller frame, the nonzero i_d helps to pull the rotor d-axis back to align with the controller d-axis. In Fig. 3, at zero speed operation, one can observe that i_q and $\hat{\theta}_d$ are slowly deviating even though the load motor outputs constant load torque. In this case, the nonzero i_d helps to "lock" the shaft at zero speed if $\theta_d\neq\hat{\theta}_d$.

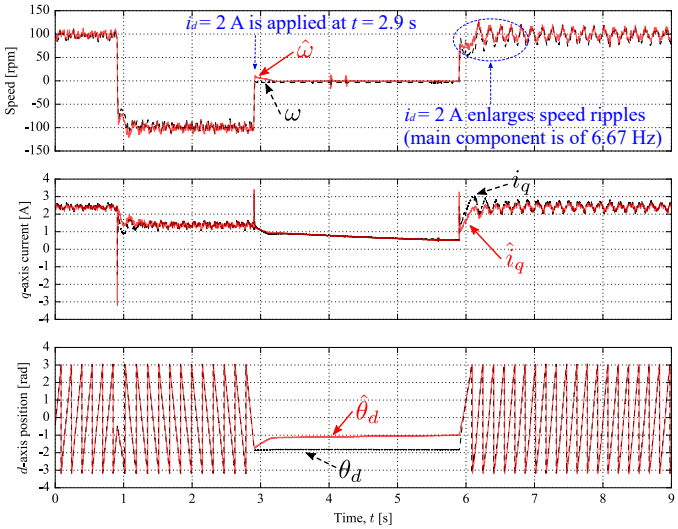

Fig. 3. Sensorless zero speed stopping test under step speed command. The flux estimator tuning is $k_p=20, k_i=4$ (all in SI units).

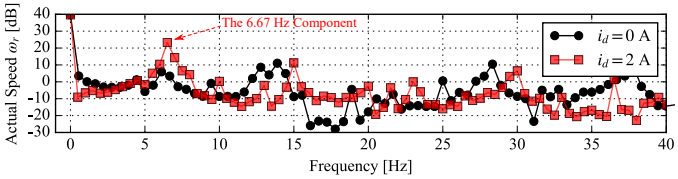

Fig. 4. Fourier analysis of the actual speed waveform from Fig. 3. Spectrum of $i_d=0$ A corresponds to $t\in(1.1, 2.9)$ s in Fig. 3, and spectrum of $i_d=2$ A corresponds to time domain data of $t\in(7, 9)$ s in Fig. 3.

In Fig. 3, the speed ripples are found to have vanished at zero speed. After applying nonzero i_d, the speed ripples become more apparent at 100 rpm, and are found to have the same frequency of the mechanical speed of 6.67 Hz (i.e., 100 rpm). This is further supported with Fourier analysis as shown in Fig. 4. When $i_d=0$ A, the average value of the actual speed is 39.8 dB (i.e., -97.2 rpm), and the amplitude of the 6.67 Hz speed harmonic is 5.9 dB; while $i_d=2$ A, the average value of the actual speed is 39.6 dB (i.e., 95.5 rpm), and the amplitude of the 6.67 Hz speed harmonic is increased to 23 dB. How to reduce the speed ripples is beyond the scope of this letter, but the thing to note here is that the speed estimate $\hat{\omega}$ even tracks the speed ripples in ω at 100 rpm steady state.

4) Sensorless Slow Speed Reversal: The point of a slow speed reversal test is to keep decreasing the acceleration rate of the ramp speed command until the sensorless drive shows some undesired behaviors. In our case, the acceleration is ±50 rpm/s in Fig. 5. At a glance, one might consider

This article has been accepted for publication in a future issue of this journal, but has not been fully edited. Content may change prior to final publication. Citation information: DOI 10.1109/TPEL.2021.3094583, IEEE Transactions on Power Electronics

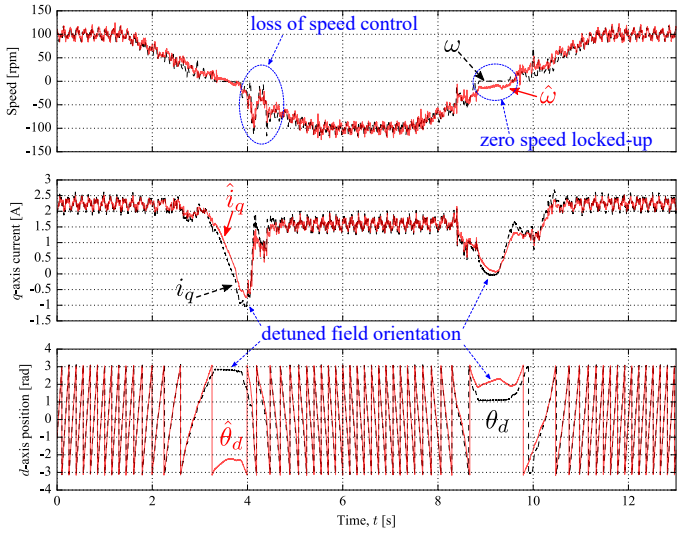

Fig. 5. Sensorless slow speed reversal test with ramping speed command and $i_d = 2$ A. The flux estimator tuning is $k_p = 20, k_i = 4$ (all in SI units).

Fig. 5 shows a successful slow speed reversal test. However, there exist problems of "zero speed locked-up", "detuned field orientation", and "loss of speed control" as annotated in Fig. 5.

Zero speed locked-up occurs when the actual motor speed ω becomes zero regardless of the speed command during speed reversal near zero speed. Detuned field orientation essentially means $\hat{\theta}_d$ from the active flux estimator deviates from θ_d. In a sensorless drive, a clear indicator for loss of field orientation is that i_q deviates from its desired value, as shown in Fig. 5, at $t = 4$ s when the motor escapes from zero speed locked-up, and at $t = 9$ s when the motor is locked up at zero speed. A severer consequence of loss of field orientation is loss of speed control at $t = 4$ s when the actual speed reaches over -100 rpm when the speed command is about -30 rpm. During loss of speed control, the actual speed diverges from speed command, but as $\hat{\theta}_d$ converges, speed control is attained again.

V. Discussion

A. Improving Slow Speed Reversal Performance

1) Integrator with Nonlinear Amplitude Limiter: In [26], an integrator with a flux amplitude limiter is proposed for flux estimation

$$p\boldsymbol{\psi}_1 = \boldsymbol{u} - R\boldsymbol{i} + k_p\left(L_{\mathrm{CM}}\frac{\boldsymbol{\psi}_2}{|\boldsymbol{\psi}_2|} - \boldsymbol{\psi}_2\right) \tag{13a}$$

$$L_{\mathrm{CM}} = \begin{cases} |\boldsymbol{\psi}_2|, & \text{if } \left|\boldsymbol{\psi}_2^{'}\right| \le K_{\mathrm{Active}} \\ K_{\mathrm{Active}}, & \text{others} \end{cases} \tag{13b}$$

where the limiter correction is only active when $|\boldsymbol{\psi}_2|$ is larger than K_{Active}, and in other words, when $|\boldsymbol{\psi}_2|$ is smaller than K_{Active}, (13a) becomes an unstable pure integrator.

2) Integrator with Linear Amplitude Correction: The integrator with limiter (13) is suitable for induction motor, but it does not make sense for PM motor whose rotor flux amplitude is always equal to K_E, so when $|\boldsymbol{\psi}_2|$ is smaller than K_{Active}, it should also be corrected. In fact, (13) becomes (9) if we put $L_{\mathrm{CM}} = K_{\mathrm{Active}}$ and $k_i = 0$. Consequently, the transfer function in (12) reduces to a first-order one, which is consistent with our tuning guideline to select a large damping ratio ζ_{est}.

3) Additional Flux Limiter Correction: The estimator dynamics (9) are modified with an additional flux limiter [17]

$$\begin{aligned} p\boldsymbol{\psi}_1' =& \boldsymbol{u} - R\boldsymbol{i} - k_{\mathrm{limiter}}\left(\boldsymbol{\psi}_2' - \boldsymbol{\psi}_{2\mathrm{limited}}'\right) \\ &+ \left(k_p + \frac{k_i}{p}\right)\left(K_{\mathrm{Active}}\frac{\boldsymbol{\psi}_2'}{|\boldsymbol{\psi}_2'|} - \boldsymbol{\psi}_2'\right) \end{aligned} \tag{14a}$$

$$\boldsymbol{\psi}_2' = \boldsymbol{\psi}_1' - L_q\boldsymbol{i} \tag{14b}$$

$$\boldsymbol{\psi}_{2\mathrm{limited}}' = \begin{cases} \boldsymbol{\psi}_2', & \text{if } |\boldsymbol{\psi}_2'| \le \kappa K_{\mathrm{Active}} \\ \kappa K_{\mathrm{Active}}\frac{\boldsymbol{\psi}_2'}{|\boldsymbol{\psi}_2'|}, & \text{others} \end{cases} \tag{14c}$$

where $\kappa = 1.15$ [17], and k_{limiter} is active and set to $2\pi \times 100$ rad/s only if the absolute value of the speed command is less than $1.5\ \mathrm{s}^{-1}$ (i.e., 90 rpm in our case). Note (14) is a combination of (9) and (13).

4) Experimental Results: More experimental results of slow speed reversal are presented in Fig. 6. In Fig. 6, both the loss of speed control and zero-speed lock-up phenomena are gone. Even though the speed waveform in Fig. 6a trends to diverge, it is pulled back to speed command before it develops oscillation. However, in Fig. 6a and 6c, a new phenomenon of *zero-speed oscillation* occurs during slow zero speed crossing (instead of speed waveform being a straight horizontal line at zero speed as in Fig. 5). Besides, the 6.67 Hz speed ripples are mitigated in Fig. 6, because i_d is regulated to 0.

In conclusion, the experimental results using (9) with $k_p = 200$ rad/s and $k_i = 0$ are preferred, as there is no speed oscillation at zero speed, and the waveforms of θ_d and $\hat{\theta}_d$ resemble that of sensored control the most.

B. Comparative Studies to EMF based Drive

A popular[4] sliding mode observer (SMO) from [4] is adopted for the comparison between the emf-based drive and flux-based drive. Corresponding successful experimental slow speed reversal results are shown in Fig. 6d, and high speed reversal results are shown in Fig. 2d. The fast switching nature of SMO causes the motor speed ripples in Fig. 6d and Fig. 2d, and we have been using a time-varying SM gain k for low speed operation to mitigate the chattering issues.

According to our studies, emf-based drive using SMO can achieve comparable performance as ours. However, it is much more complicated to tune. Particularly, implementing SMO needs to tune an SM gain, a speed dependent low pass filter pole, and a coefficient to mitigate chattering of switching function (e.g., saturation function in [4] or sigmoid function in [8], [16]), in order to get rotor position, while (9) needs to tune only one parameter, i.e., ω_{est} for high speed, or only k_p for extreme low speed. Specifically, during low speed operation, the tuning is as simple as increasing k_p until it stabilizes the pure integrator, and moreover, choosing a large k_p does not bring penalty to system performance, i.e., no chattering issues.

VI. Conclusion

After categorizing existing sensorless drives into groups of three design patterns, this letter proposes a simple load torque-adaptive natural speed observer using the active flux concept,

[4]For example, it is later adopted in [27] to reconstruct extended emf.

This article has been accepted for publication in a future issue of this journal, but has not been fully edited. Content may change prior to final publication. Citation information: DOI 10.1109/TPEL.2021.3094583, IEEE Transactions on Power Electronics

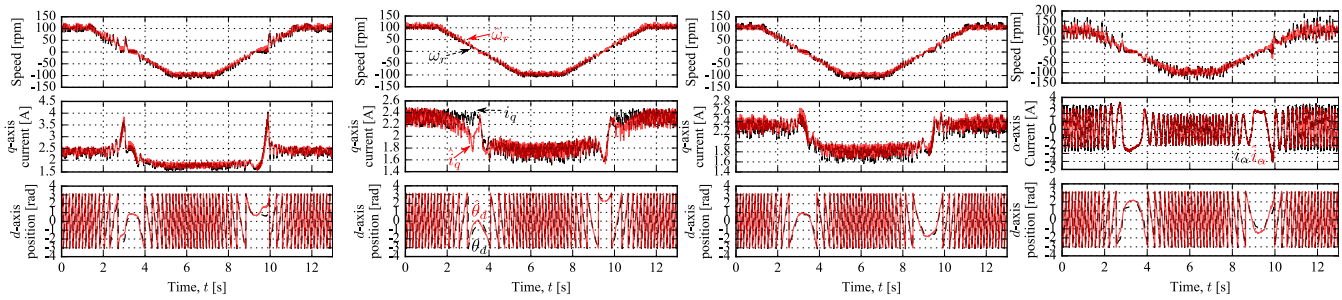

Fig. 6. Sensorless slow speed reversal test (a) using (13) with $k_p = 200$; (b) using (9) with $k_p = 200$, $k_i = 0$; (c) using (14) with $\omega_{\rm est} = 2$ and $\zeta_{\rm est} = 5$ (all in SI units); (d) using SMO, with $k = 10K_E\,|\omega^*| + 5$ V and $\tau_c^{-1} = 5$ rad/s, where k and τ_c are defined in [4].

which follows the third design pattern. The experimental results show improved performance in slow speed reversal, as compared to existing sensorless drive that follows second design pattern [12], and existing emf-based drive using SMO. High speed fast reversal and loaded zero speed operation are also found possible. The tuning of the proposed drive is as simple as tuning two parameters, one for position estimation and the other for speed estimation.

This letter proposes a new dynamic expression for the active flux, and by introducing the active flux concept, the proposed sensorless design is applicable to different types of ac electric motors. It is worth pointing out that the slow speed reversal test done by a natural speed observer based sensorless induction motor drive can go down to 5 rpm/s acceleration using a four pole motor [23].

REFERENCES

[1] Z. Chen, M. Tomita, S. Doki, and S. Okuma, "An extended electromotive force model for sensorless control of interior permanent-magnet synchronous motors," *IEEE Transactions on Industrial Electronics*, vol. 50, no. 2, pp. 288–295, Apr 2003.

[2] L. Harnefors, M. Jansson, R. Ottersten, and K. Pietilainen, "Unified sensorless vector control of synchronous and induction motors," *IEEE Transactions on Industrial Electronics*, vol. 50, no. 1, pp. 153–160, 2003.

[3] I. Boldea, M. C. Paicu, and G. Andreescu, "Active flux concept for motion-sensorless unified ac drives," *IEEE Transactions on Power Electronics*, vol. 23, no. 5, pp. 2612–2618, 2008.

[4] S. Chi, Z. Zhang, and L. Xu, "Sliding-mode sensorless control of direct-drive pm synchronous motors for washing machine applications," *IEEE Transactions on Industry Applications*, vol. 45, no. 2, pp. 582–590, 2009.

[5] R. Ortega, L. Praly, A. Astolfi, J. Lee, and K. Nam, "Estimation of rotor position and speed of permanent magnet synchronous motors with guaranteed stability," *IEEE Transactions on Control Systems Technology*, vol. 19, no. 3, pp. 601–614, 2011.

[6] N. Matsui, "Sensorless pm brushless dc motor drives," *IEEE Transactions on Industrial Electronics*, vol. 43, no. 2, pp. 300–308, April 1996.

[7] P. Jansen and R. Lorenz, "Accuracy limitations of velocity and flux estimation in direct field oriented induction machines," in *1993 fifth European conference on power electronics and applications*. IET, 1993, pp. 312–318.

[8] Z. Qiao, T. Shi, Y. Wang, Y. Yan, C. Xia, and X. He, "New sliding-mode observer for position sensorless control of permanent-magnet synchronous motor," *IEEE Transactions on Industrial Electronics*, vol. 60, no. 2, pp. 710–719, Feb 2013.

[9] C. J. Volpato Filho and R. P. Vieira, "Adaptive full-order observer analysis and design for sensorless interior permanent magnet synchronous motors drives," *IEEE Transactions on Industrial Electronics*, pp. 1–1, 2020.

[10] J. Chen, J. Huang, and Y. Sun, "Resistances and speed estimation in sensorless induction motor drives using a model with known regressors," *IEEE Transactions on Industrial Electronics*, vol. 66, no. 4, pp. 2659–2667, April 2019.

[11] J. Chen and J. Huang, "Application of adaptive observer to sensorless induction motor via parameter-dependent transformation," *IEEE Transactions on Control Systems Technology*, vol. 27, no. 6, pp. 2630–2637, Nov 2019.

[12] M. Jansson, L. Harnefors, O. Wallmark, and M. Leksell, "Synchronization at startup and stable rotation reversal of sensorless nonsalient pmsm drives," *IEEE Transactions on Industrial Electronics*, vol. 53, no. 2, pp. 379–387, 2006.

[13] M. Hinkkanen, T. Tuovinen, L. Harnefors, and J. Luomi, "A combined position and stator-resistance observer for salient pmsm drives: Design and stability analysis," *IEEE Transactions on Power Electronics*, vol. 27, no. 2, pp. 601–609, 2012.

[14] H. Tajima, Y. Matsumoto, and H. Umida, "Speed sensorless vector control method for an industrial drive system," *IEEJ Transactions on Industry Applications*, vol. 116, no. 11, pp. 1103–1109, 1996.

[15] S. Sul, Y. Kwon, and Y. Lee, "Sensorless control of ipmsm for last 10 years and next 5 years," *CES Transactions on Electrical Machines and Systems*, vol. 1, no. 2, pp. 91–99, 2017.

[16] H. Kim, J. Son, and J. Lee, "A high-speed sliding-mode observer for the sensorless speed control of a pmsm," *IEEE Transactions on Industrial Electronics*, vol. 58, no. 9, pp. 4069–4077, Sept 2011.

[17] Y. Park and S. K. Sul, "Sensorless control method for pmsm based on frequency-adaptive disturbance observer," *IEEE Journal of Emerging and Selected Topics in Power Electronics*, vol. 2, no. 2, pp. 143–151, June 2014.

[18] B. Yi, S. N. Vukosavić, R. Ortega, A. M. Stanković, and W. Zhang, "A frequency domain interpretation of signal injection methods for salient pmsms," in *2019 IEEE Conference on Control Technology and Applications (CCTA)*. IEEE, 2019, pp. 517–522.

[19] H.-S. Kim, S.-K. Sul, H. Yoo, and J. Oh, "Distortion-Minimizing Flux Observer for IPMSM Based on Frequency-Adaptive Observers," *IEEE Transactions on Power Electronics*, vol. 35, no. 2, pp. 2077–2087, Feb. 2020.

[20] J. Yoo, H.-S. Kim, and S.-K. Sul, "Design of frequency-adaptive flux observer in pmsm drives robust to discretization error," *IEEE Transactions on Industrial Electronics*, pp. 1–1, 2021.

[21] A. Piippo, M. Hinkkanen, and J. Luomi, "Analysis of an adaptive observer for sensorless control of interior permanent magnet synchronous motors," *IEEE Transactions on Industrial Electronics*, vol. 55, no. 2, pp. 570–576, 2008.

[22] T. A. Lipo, *Analysis of synchronous machines*. CRC Press, 2012.

[23] J. Chen and J. Huang, "Alternative solution regarding problems of adaptive observer compensating parameters uncertainties for sensorless induction motor drives," *IEEE Transactions on Industrial Electronics*, vol. 67, no. 7, pp. 5879–5888, July 2020.

[24] S. R. Bowes, A. Sevinc, and D. Holliday, "New natural observer applied to speed-sensorless dc servo and induction motors," *IEEE Transactions on Industrial Electronics*, vol. 51, no. 5, pp. 1025–1032, Oct 2004.

[25] J. Chen and J. Huang, "Online decoupled stator and rotor resistances adaptation for speed sensorless induction motor drives by a time-division approach," *IEEE Transactions on Power Electronics*, vol. 32, no. 6, pp. 4587–4599, June 2017.

[26] J. Hu and B. Wu, "New integration algorithms for estimating motor flux over a wide speed range," *IEEE Transactions on Power Electronics*, vol. 13, no. 5, pp. 969–977, Sep 1998.

[27] G. Wang, R. Yang, and D. Xu, "Dsp-based control of sensorless ipmsm drives for wide-speed-range operation," *IEEE Transactions on Industrial Electronics*, vol. 60, no. 2, pp. 720–727, 2012.